030601-12-T

AWE TECHNIQUES IN FREQUENCY DOMAIN ELECTROMAGNETICS

Y. E. Erdemli
C.J. Reddy
J.L. Volakis

National Aeronautics and
Space Administration
Langley Research Center
Hampton, VA 23681-0001

January 1997

30601-12-T = RL-2431

PROJECT INFORMATION

PROJECT TITLE: Simulation of Conformal Spiral Antennas on Composite Platforms

REPORT TITLE: AWE Techniques in Frequency Domain Electromagnetics

U-M REPORT No.: 030601-12-T

CONTRACT
START DATE: January 1993
END DATE: December 1997

DATE: January 1998

SPONSOR: Fred Beck
NASA Langley Research Center
M/S 490
Hampton, VA 23681
Phone: (804)864-1829

Grant No. NAG 1-1478

U-M PRINCIPAL
INVESTIGATOR: John L. Volakis
EECS Dept.
University of Michigan
1301 Beal Ave
Ann Arbor, MI 48109-2122
Phone: (734) 764-0500 FAX: (734) 747-2106
volakis@umich.edu
http://www-personal.engin.umich.edu/~volakis/

CONTRIBUTORS
TO THIS REPORT: Y. E. Erdemli (UM), C.J. Reddy (Hampton Univ.)
J. Volakis(UM).

AWE Technique in Frequency Domain Electromagnetics

Yunus E. Erdemli[*], C.J.Reddy[#] and John L. Volakis[*]

Abstract:

This paper presents fast radar cross section (RCS) computations using the Asymptotic Waveform Evaluation (AWE) technique in conjunction with Method of Moments (MoM) and hybrid Finite Element (FEM/MoM) implementations. In its traditional form, AWE constructs a reduced-order model of a given linear system by Taylor series expansion with respect to specific values of the system parameters (frequency, angle, etc.). Thus, AWE permits the prediction of the frequency response from a few frequency calculations. In this paper we modify AWE to instead employ a rational function (Padè approximation) representation for the system parameters. Using a Padè rational function instead of a Taylor series, the accuracy of the analysis is increased to a wider frequency range. AWE is also extended to allow monostatic RCS pattern prediction using again a few pattern values, thus eliminating a need to resolve the system when an iterative solver is employed. To demonstrate these extensions of AWE, numerical examples of three-dimensional metallic bodies and cavity-backed apertures are considered.

[*] Y. E. Erdemli and J.L. Volakis are with Radiation Laboratory, University of Michigan, Ann Arbor MI, USA.

[#] C. J. Reddy is with Department of Electrical Engineering, Hampton University, Hampton VA 23668, USA.

1. Introduction

Numerical methods such as the Method of Moments (MoM), Finite Element Method (FEM) and hybrid FEM/MoM techniques have gained wide acceptance due to their flexibility to model arbitrarily shaped objects involving complex materials [1,2]. In all these methods, a matrix system is formed and solved to obtain the desired system parameters using a direct or an iterative solver. For electrically large problems, the solution of the matrix system is computationally intensive and must be repeated for each frequency. Also, certain analyses and designs may require both temporal and frequency responses placing additional computational burden in generating these responses. To speed-up computations for large-scale simulations, iterative techniques which incorporate fast algorithms such as the Fast Multipole Method (FMM) and Adaptive Integral Method (AIM) [3,4] have been introduced. When incorporated into MoM or hybrid FEM/MoM codes, these algorithms have allowed the solution of practical problems [5-7]. However, the solution must be independently carried out for each excitation (incidence angle). Monostatic RCS calculations are therefore computationally intensive and therefore for iterative methods, asymptotic waveform evaluation (AWE) or the extrapolation methods become attractive for CPU reduction.

In this paper, we investigate the application of AWE in conjunction with MoM and hybrid FEM/MoM techniques for rapid frequency response calculations. We also present a new implementation of AWE for rapid monostatic pattern fill calculations when an iterative solver is employed.

AWE provides a reduced-order model of a linear system that has already been successfully used in VLSI and circuit analyses to approximate the transfer function

associated with circuit networks [8,9]. We note that a similar method was used by Burke et al [10,11] under the name of Model Based Parameter Estimation (MBPE). Both AWE and MBPE are identical in nature. The AWE technique has also been applied for FEM based problems by Gong et al [12] and Polstyanko et al [13] used AWE for the efficient analysis of dielectric waveguides.

In this paper, a detailed analysis of AWE applied to hybrid frequency domain EM techniques is presented for the first time. We also extend AWE to include a rapid monostatic pattern fill in the case of large problems which invariably depend on iterative solvers. In the AWE technique, the unknown variable (electric field/current) is expanded in a Taylor series about the frequency or angle. These moments of the Taylor series are then mapped to a Padè approximation. The latter has a much larger range of convergence. Thus, it provides a larger frequency or angular region of extrapolation.

This paper is organized as follows. In section 2, the AWE implementation for MoM and the combined FEM/MoM technique is presented for obtaining a frequency response. The AWE procedure for monostatic RCS fill using iterative techniques is also described in section 2. Numerical results for various examples are presented in section 3.

2. Formulation

AWE is an extrapolation approach which provides a reduced-order model of a linear system. On the basis of AWE, a Taylor series expansion of the matrix system (MoM or FEM/MoM) is generated about a specific value of the system parameter (frequency, angle etc.). The Taylor coefficients or moments are then used to extract poles and residues of the system yielding a rational function (Padè approximation) of the system

parameter. Padè representations have a larger circle of convergence and can therefore provide a broader extrapolation since it includes poles as well as zeros of the response. This representation provides an extension of the region of convergence (RoC) of the power series, thus increasing the accuracy of the analysis to a wider range.

2.1 Asymptotic Waveform Evaluation (AWE)

To illustrate the AWE method, let us consider a one-variable complex function $f(z)$. The Taylor series of $f(z)$ at z_0 is

$$f(z) = \sum_{n=0}^{\infty} c_n (z - z_0)^n \ , \ c_0 = f(z_0) \ , \tag{1a}$$

$$c_n = \frac{f^{(n)}(z_0)}{n!} \ , \ f^{(n)}(z_0) = \left. \frac{d^n f(z)}{dz^n} \right|_{z=z_0} \ . \tag{1b}$$

This expansion is the basic starting point for the Padè approximation given by

$$P(L/M) \equiv \frac{\sum_{l=0}^{L} a_l (z - z_0)^l}{1 + \sum_{m=1}^{M} b_m (z - z_0)^m} = \frac{Q_L(z)}{1 + R_M(z)} \tag{2}$$

in which L and M are the orders of the zero and pole expansions. The coefficients a_l and b_m of the numerator (Q_L) and denominator (R_M) polynomials, respectively, are found by enforcing equality of (1) and (2), viz.,

$$\sum_{n=0}^{\infty} c_n (z - z_0)^n = \frac{\sum_{l=0}^{L} a_l (z - z_0)^l}{1 + \sum_{m=1}^{M} b_m (z - z_0)^m} + O(z^{L+M+1}) \ . \tag{3}$$

Upon cross-multiplying and equating equal powers of z in equation (3), we get the linear system [14]

$$\begin{pmatrix} c_{L-M+1} & c_{L-M+2} & c_{L-M+3} & \cdots & c_L \\ c_{L-M+2} & c_{L-M+3} & c_{L-M+4} & \cdots & c_{L+1} \\ c_{L-M+3} & c_{L-M+4} & c_{L-M+5} & \cdots & c_{L+2} \\ \vdots & \vdots & \vdots & \ddots & \vdots \\ c_L & c_{L+1} & c_{L+2} & \cdots & c_{L+M-1} \end{pmatrix} \begin{pmatrix} b_M \\ b_{M-1} \\ b_{M-2} \\ \vdots \\ b_1 \end{pmatrix} = - \begin{pmatrix} c_{L+1} \\ c_{L+2} \\ c_{L+3} \\ \vdots \\ c_{L+M} \end{pmatrix} \tag{4}$$

which is of order M. This system refers only to higher powers of z, in particular z^i with $i=L+1,L+2,\ldots,L+M$. As a result, all equations involving a_l are eliminated. The a_l coefficients are found after solution of (4) for b_m and by equating powers of z less than $L+1$, giving [14]

$$a_0 = c_0 \ , \ a_1 = c_1 + b_1 c_0 \ , \ a_2 = c_2 + b_1 c_1 + b_2 c_0 \ , \ldots , \ a_L = c_L + \sum_{j=1}^{\min(L,M)} b_j c_{L-j} \ . \tag{5}$$

Typically, there exist optimum values for L and M so that a Padè representation $P^{opt}(L/M)$ best approximate $f(z)$ around z_0.

Below we first describe the implementation of AWE into MoM for frequency extrapolation and monostatic pattern fill. We then proceed with a similar implementation for hybrid FEM/MoM systems.

2.2 Method of Moments (MoM)

MoM is a popular tool for accurate prediction of radar cross section (RCS) calculations. Its implementation in connection with the Electric Field Integral Equation (EFIE) involves a solution of the electric current surface density using a direct or some

iterative solver. With frequency (f) as the parameter of interest for extrapolation, the discretized EFIE [15] results in the linear system

$$[Z_{mn}(k)]_{N\times N}\{I_n(k;\phi,\theta)\}_{N\times 1} = \{V_m(k;\phi,\theta)\}_{N\times 1} \ , \tag{6a}$$

$$Z_{mn}(k) = jk\eta_0 \iint \mathbf{T}_m \cdot \iint \mathbf{T}_n G_k(R)\, ds'ds - \frac{j\eta_0}{k} \iint (\nabla\cdot\mathbf{T}_m) \iint (\nabla'\cdot\mathbf{T}_n)\, G_k(R)\, ds'ds \ , \tag{6b}$$

$$V_m(k;\phi,\theta) = \iint \mathbf{T}_m \cdot \mathbf{E}_{inc}(k;\phi,\theta)\, ds \ , \ \mathbf{E}_{inc}(k;\phi,\theta) = \mathbf{p}_i\, e^{j\mathbf{k}\cdot\mathbf{r}} \ , \tag{6c}$$

$$\mathbf{r} = \hat{x}x + \hat{y}y + \hat{z}z \ , \ R = \left|\mathbf{r}-\mathbf{r}'\right| = \sqrt{(x-x')^2+(y-y')^2+(z-z')^2} \ , \tag{6d}$$

$$\begin{aligned}\mathbf{p}_i = {} & \hat{x}(\cos\theta\cos\phi\cos\alpha - \sin\phi\sin\alpha) + \\ & \hat{y}(\cos\theta\sin\phi\cos\alpha - \cos\phi\sin\alpha) - \hat{z}\sin\theta\cos\alpha \ ,\end{aligned} \tag{6e}$$

$$\mathbf{k} = (-\hat{x}\sin\theta\cos\phi + \hat{y}\sin\theta\sin\phi + \hat{z}\cos\theta)k \ , \ k = 2\pi f\sqrt{\mu_0\varepsilon_0} \ , \ G_k(R) \equiv \frac{e^{-jkR}}{4\pi R} \tag{6f}$$

where we have expanded the unknown current density as

$$\mathbf{J}(\mathbf{r}) = \sum_{n=1}^{N} I_n(k;\phi,\theta)\, \mathbf{T}_n(\mathbf{r}) \tag{7}$$

in which $\mathbf{T}_n(\mathbf{r})$ denotes the subsectional basis function. Among the other parameters, $V(k;\phi,\theta)$ is the excitation vector and $Z_{mn}(k)$ represents the weighted integral used for generating the matrix. $I_n(k;\phi,\theta)$ is the unknown current and N is the number of unknowns. Also, $\mathbf{E}_{inc}$ denotes the incident electric field; $\mathbf{p}_i$ is the unit vector representing the direction of the incident electric field; (ϕ,θ) is the incidence angle; α is the polarization angle; $\mathbf{k}$ represents the propagation direction of the incident wave; η_0 is the intrinsic impedance of the medium; $\mathbf{r}$ and $\mathbf{r}'$ are the vectors defining the observation and source points, respectively, and R is the distance between these two locations.

Equation (6a) is typically solved at a specific frequency f_0 (with wavenumber k_0) either by a direct or an iterative method. The advantage of a direct method is that $[Z_{mn}(k_0)]$ needs to be decomposed or inverted only once and subsequently the much less CPU intensive forward/backward substitutions (LU decomposition) are performed to obtain the solution for $\mathbf{J}(k_0;\phi,\theta)$ for each excitation. However, if **J** or the RCS response is needed over a frequency band, the evaluation of $[Z_{mn}(k)]$ and its decomposition must be carried out repeatedly at each frequency. Since this may be an $O(N^3)$ operation for each frequency point, use of frequency extrapolation techniques, such as AWE, are very attractive for CPU reduction.

2.2.a Frequency Extrapolation

In this section we introduce AWE to evaluate $I_n(k;\phi,\theta)$ at multiple frequency points. We begin by expanding $\{I_n(k)\}$ as

$$\{I_n(k)\}_{N\times 1} = \sum_{s=0}^{\infty} \{M_n^s\}_{N\times 1}(k-k_0)^s \ , \ M_n^s = \frac{I_n^{(s)}(k_0)}{s!} \ , \ I_n^{(s)}(k_0) = \left.\frac{d^s I_n(k)}{dk^s}\right|_{k=k_0} . \tag{8}$$

The "moments" $\{M^s_n\}$ can be evaluated in closed form using the relation

$$\{M_n^s\} = [Z_{mn}(k_0)]^{-1}\left[\frac{\{V_m^{(s)}(k_0)\}}{s!} - \sum_{q=0}^{s}\frac{(1-\delta_{q0})[Z_{mn}^{(q)}(k_0)]\{M_n^{s-q}\}}{q!}\right], \tag{9a}$$

$$V_m^{(s)}(k_0) = \left.\frac{d^s V_m(k)}{dk^s}\right|_{k=k_0} \ , \ Z_{mn}^{(q)}(k_0) = \left.\frac{d^q Z_{mn}(k)}{dk^q}\right|_{k=k_0} \ , \ \delta_{q0} = \begin{cases} 1 & q=0 \\ 0 & q\neq 0 \end{cases} . \tag{9b}$$

Here $Z^{(q)}_{mn}(k)$ is the q^{th} derivative of $Z_{mn}(k)$ with respect to k. This evaluation is unfortunately a lengthy process but requires much less time than a direct decomposition of $[Z_{mn}(k)]$. Actually, the derivatives can be obtained by successive differentiation of the

previous derivatives of $Z_{mn}(k)$. It can be shown that an explicit and compact representation of $Z^{(q)}_{mn}(k)$ is

$$Z^{(q)}_{mn}(k) = jk\eta_0 \iint \mathbf{T}_m \cdot \iint \mathbf{T}_n \, (-jR)^q \left(1 - \frac{q}{jkR}\right) G_k(R)\, ds'ds$$
$$- \frac{j\eta_0}{k} \iint (\nabla \cdot \mathbf{T}_m) \iint (\nabla' \cdot \mathbf{T}_n)(-jR)^q \left(\sum_{p=0}^{q} \frac{q!}{(q-p)!(jkR)^p} \right) G_k(R)\, ds'ds \ . \tag{10}$$

Similarly, the expression for the s^{th} derivative of $V_n(k)$ with respect to k is readily given by

$$V^{(s)}_m(k) = \iint \mathbf{T}_m \cdot \mathbf{p}_i (j\mathbf{k} \cdot \mathbf{r})^s \, e^{j\mathbf{k}\cdot\mathbf{r}} ds \ . \tag{11}$$

Substituting equations (10) and (11) in (9a), we generate the AWE moments. These moments are subsequently introduced into (8) to yield $\{I_n(k)\}$ at frequency points around k_0. Note that this process requires the decomposition of $[Z_{mn}(k)]$ only at the reference frequency k_0. However, the accuracy of (8) quickly deteriorates as k moves away from k_0. Thus, we instead consider an alternative expansion based on Padè approximants.

The Padè approximation can be obtained by using the procedure described in section 2.1. Each entry of the vector $\{I_n(k)\}_{N\text{x}1}$ in (8) can be thought of as a complex function of k and can be expanded as

$$I_n(k) \equiv \sum_{s=0}^{\infty} M_n^s (k - k_0)^s \ . \tag{12}$$

Using this notation, the Padè representation for each $I_n(k)$ (n=1, 2, …, N) is then given by

$$P_n(L/M) = \frac{\sum_{l=0}^{L} a_n^l (k - k_0)^l}{1 + \sum_{m=1}^{M} b_n^m (k - k_0)^m} \ , \tag{13a}$$

$$\sum_{s=0}^{\infty} M_n^s (k - k_0)^s = P_n(L/M) + O(k^{L+M+1}) \ . \tag{13b}$$

The unknown coefficients, a^l_n and b^m_n appearing in the Padè approximation satisfy the linear system

$$\sum_{j=1}^{l} M_n^{l-j} b_n^j = -M_n^l \ , \ L+1 \le l \le L+M \ , \ l > M : b_n^j = 0 \ , \tag{14a}$$

$$a_n^0 = M_n^0 \ , \ a_n^l = \sum_{j=1}^{l} M_n^{l-j} b_n^j \ , \ 1 \le l \le L \ , \ 1 \le n \le N \ , \tag{14b}$$

and these are similar relations to those found in (4) and (5) but stated in a different manner. The Padè coefficients are determined from a solution of (14). We can write

$$\{I_n(k)\}_{N\times 1} \cong \{P_n(L/M)\}_{N\times 1} \ . \tag{15}$$

2.2.b Pattern Fill

For monostatic pattern evaluations it is necessary to carry out the matrix vector product $[Z_{mn}(k)]^{-1}\{V_m(\phi,\theta)\}$ for each excitation $\{V_m(\phi,\theta)\}$. AWE can again be employed for calculating the angular variations of a monostatic pattern using only a few pattern points, thus eliminating a need to carry out the backsubstitution repetitively. For iterative solvers, the proposed pattern fill procedure eliminates repetition of the iterative solutions altogether except for a few pattern points.

To show how AWE can be applied, we begin by restating the system

$$\{I_n(\phi,\theta)\}_{N\times 1} = [Z_{mn}(k_0)]^{-1}_{N\times 1} \{V_m(\phi,\theta)\}_{N\times 1} \tag{16}$$

where we observe that $[Z_{mn}(k_0)]^{-1}$ is not a function of the incidence or observation angles. Assume now that $\{I_n(\phi,\theta)\}$ has already been computed at a given direction (ϕ_0,θ_0). Thus, we can use a Taylor series to express $I_n(\phi,\theta)$ as

$$I_n(\phi,\theta) = I_n(\phi_0,\theta_0) + \left.\frac{\partial I_n(\phi,\theta)}{\partial\phi}\right|_{\substack{\phi=\phi_0\\ \theta=\theta_0}} (\phi-\phi_0) + \left.\frac{\partial I_n(\phi,\theta)}{\partial\theta}\right|_{\substack{\phi=\phi_0\\ \theta=\theta_0}} (\theta-\theta_0) + \frac{1}{2!}\left.\frac{\partial^2 I_n(\phi,\theta)}{\partial\phi^2}\right|_{\substack{\phi=\phi_0\\ \theta=\theta_0}} (\phi-\phi_0)^2$$

$$+ \frac{1}{2!}\left.\frac{\partial^2 I_n(\phi,\theta)}{\partial\theta^2}\right|_{\substack{\phi=\phi_0\\ \theta=\theta_0}} (\theta-\theta_0)^2 + \frac{1}{2!}\left.\frac{\partial^2 I_n(\phi,\theta)}{\partial\phi\partial\theta}\right|_{\substack{\phi=\phi_0\\ \theta=\theta_0}} (\phi-\phi_0)(\theta-\theta_0) + \ldots \qquad (17)$$

Next upon making use of (16) we can eliminate the derivatives of $I_n(\phi,\theta)$ to obtain the more explicit expression

$$\{I_n(\phi,\theta)\} = [Z_{mn}(k_0)]^{-1}\left\{\{V_m(\phi_0,\theta_0)\} + \sum_{q=1}^{\infty}\frac{1}{q!}\left[\{V^{(q)}_{m(\phi)}(\phi_0,\theta_0)\}(\phi-\phi_0)^q\right.\right.$$
$$\left.\left. + \{V^{(q)}_{m(\theta)}(\phi_0,\theta_0)\}(\theta-\theta_0)^q\right] + \sum_{p=1}^{\infty}\sum_{s=1}^{\infty}\frac{1}{(p+s)!}\{V^{(p+s)}_{m(\phi\theta)}(\phi_0,\theta_0)\}(\phi-\phi_0)^p(\theta-\theta_0)^s\right\}, \qquad (18a)$$

$$V^{(q)}_{m(\psi)}(\phi_0,\theta_0) \equiv \left.\frac{\partial^q V_m(\phi,\theta)}{\partial\psi^q}\right|_{\substack{\phi=\phi_0\\ \theta=\theta_0}} (\psi=\phi \text{ or } \theta)\ ,\ V^{(p+s)}_{m(\phi\theta)}(\phi_0,\theta_0) \equiv \left.\frac{\partial^{(p+s)} V_m(\phi,\theta)}{\partial\phi^p\partial\theta^s}\right|_{\substack{\phi=\phi_0\\ \theta=\theta_0}}. \qquad (18b)$$

Note that the differentiations have now been transformed to the excitation column since $[Z_{mn}(k_0)]$ is by its nature independent of (ϕ,θ). For one-dimensional calculations, the dependence in ϕ can be further eliminated giving

$$\{I_n(\theta)\} = [Z_{mn}(k_0)]^{-1}\left\{\{V_m(\theta_0)\} + \sum_{q=1}^{\infty}\frac{1}{q!}\{V^{(q)}_m(\theta_0)\}(\theta-\theta_0)^q\right\},\ V^{(q)}_m(\theta_0) \equiv \left.\frac{d^q V_m(\theta)}{d\theta^q}\right|_{\theta=\theta_0}. \qquad (19)$$

As an example, let us consider the case of an incident plane wave with

$$\mathbf{E}_{inc}(\theta) = \hat{y}\,F(\theta)\ ,\ F(\theta) = e^{jk_0 x\sin\theta}\ , \qquad (20)$$

obtained from (6c) by setting $\alpha = 90^\circ$ and $\phi = 0^\circ$. Inserting this into the expression for $V_m(\theta)$ in (6c) yields the excitation vector whose q^{th} derivative is needed in (19). We have

$$V^{(q)}_m(\theta_0) = \iint \mathbf{T}_m \cdot \hat{y}\,F^{(q)}(\theta_0)\,ds\ ,\ F^{(q)}(\theta_0) \equiv \left.\frac{d^q F(\theta)}{d\theta^q}\right|_{\theta=\theta_0}, \qquad (21a)$$

$$F^{(q)}(\theta_0) = jk_0 x \sum_{p=0}^{q-1} S^{(q-p)}(\theta_0) F^{(p)}(\theta_0) C_{q-1}^{p} \ , \tag{21b}$$

$$C_{q-1}^{p} \equiv \frac{(q-1)!}{p!(q-1-p)!} \quad (q \geq 1) \ , \ j = \sqrt{-1} \ , \tag{21c}$$

$$S(\theta_0) = \sin\theta_0 \ , \ S^{(q-p)}(\theta_0) = \mathrm{Re}\left\{j^{q-p}\right\}\sin\theta_0 + \mathrm{Im}\left\{j^{q-p}\right\}\cos\theta_0 \ . \tag{21d}$$

Substituting these derivatives into (19), $\{I_n(\theta)\}$ can be expressed in terms of the AWE moments $\{M^q_n\}$ as

$$\{I_n(\theta)\} = [Z_{mn}(k_0)]^{-1}\{V_m(\theta_0)\} + \sum_{q=1}^{\infty}\{M_n^q\}(\theta-\theta_0)^q \ , \ \{M_n^q\} = \frac{1}{q!}[Z_{mn}(k_0)]^{-1} V_m^{(q)}(\theta_0) \ . \tag{22}$$

Note that the moments $\{M^q_n\}$ can now be trivially calculated and therefore one could increase the order of the expansion as needed to extend the validity of the approximation to a greater angular sector. Moreover, the Padè representation of $\{I_n(\theta)\}$ can instead be used to ensure better convergence. In this case equations (12)-(15) are applicable provided k is replaced by k_0 and θ by θ_0.

2.3 Hybrid Method: FEM/MoM

Being a frequency domain analysis, the hybrid FEM/MoM technique may not be appealing for broadband frequency computations. To obtain, for example, the frequency-dependent antenna parameters, it is necessary to execute the analysis at very fine frequency increments. Needless to mention, this is a computationally intensive procedure which may be avoided using AWE.

In this section, we describe how AWE can be applied to calculate the parameters of a cavity-backed aperture antenna over a band of frequencies using the combined

FEM/MoM technique. Although the hybrid analysis presented in this paper is not restricted to any specific input feed structure, we only present the formulation for the coaxial line feed structure as shown in Figure 10.

In accordance with the FEM/MoM procedure [16] the cavity-backed antenna in Figure 10 is formulated using the finite element method for the fields within the cavity and the boundary integral for mesh truncation across the aperture. For the fields within the cavity, we enforce the "weak form" of the equations, giving

$$\iiint_V (\nabla \times \mathbf{T}) \cdot \left(\frac{1}{\mu_r} \nabla \times \mathbf{E} \right) dv - k^2 \varepsilon_r \iiint_V \mathbf{T} \cdot \mathbf{E}\, dv - j\omega\mu_0 \iint_{S_{ap}} (\mathbf{T} \times \hat{\mathbf{n}}) \cdot \mathbf{H}_{ap}\, ds = j\omega\mu_0 \iint_{S_{inp}} \mathbf{T} \cdot (\hat{\mathbf{n}} \times \mathbf{H}_{inp})\, ds \,. \tag{23}$$

Here, $\mathbf{T}$ is the vector testing function, V is the cavity volume, $\mathbf{H}_{ap}$ and $\mathbf{H}_{inp}$ are the magnetic fields at the aperture surface S_{ap} and at the input surface S_{inp}, respectively, and $\hat{\mathbf{n}}$ represents the outward unit normal for each surface; ε_r and μ_r denote, respectively, the relative permittivity and permeability of the cavity filling. For a solution of $\mathbf{E}$ using (23), it is necessary to eliminate $\mathbf{H}_{ap}$ and $\mathbf{H}_{inp}$. For $\mathbf{H}_{ap}$, this is done by introducing the integral equation

$$j\omega\mu_0 \iint_{S_{ap}} (\mathbf{T} \times \mathbf{n}) \cdot \mathbf{H}_{ap}\, ds = 2k^2 \iint_{S_{ap}} \mathbf{T}_s \cdot \left(\iint_{S_{ap}} \mathbf{M}\, G_k(R)\, ds' \right) ds - 2 \iint_{S_{ap}} (\nabla \cdot \mathbf{T}_s) \left(\iint_{S_{ap}} (\nabla' \cdot \mathbf{M})\, G_k(R)\, ds' \right) ds \,, \tag{24a}$$

$$\mathbf{T}_s = \mathbf{T} \times \hat{\mathbf{n}} \,,\; G_k(R) = \frac{e^{-jkR}}{4\pi R} \,,\; k = 2\pi f \sqrt{\varepsilon_0 \varepsilon_r \mu_0 \mu_r} \,,\; \mathbf{M} = \mathbf{E} \times \hat{z} \tag{24b}$$

proving a relation between $\mathbf{E}$ and $\mathbf{H}$ on the aperture.

To eliminate $\mathbf{H}_{inp}$, we assume that only the dominant TEM mode and its reflection exist at the coaxial cable aperture S_{inp}. That is, the electric field across S_{inp} can be expressed as

$$\mathbf{E}_{inp} = \mathbf{e}_{inc}\, e^{-jk\sqrt{\varepsilon_{rc}}z} + \mathbf{e}_{ref}\, e^{jk\sqrt{\varepsilon_{rc}}z} \ , \tag{25a}$$

$$\mathbf{e}_{inc} = \frac{\hat{\rho}}{\rho}\left(1\Big/\sqrt{2\pi\left(\frac{r_2}{r_1}\right)}\right) \ , \ \hat{\rho} = \hat{x}\cos\phi + \hat{y}\sin\phi \ , \ \rho = \sqrt{x^2+y^2} \ , \tag{25b}$$

$$\mathbf{e}_{ref} = \Gamma_0\, \mathbf{e}_{inc} \ , \ \Gamma_0 = \left\{ \frac{e^{-jk\sqrt{\varepsilon_{rc}}z_1}}{\sqrt{2\pi\ln(r_2/r_1)}} \iint_{S_{inp}} \mathbf{E}\cdot\left(\frac{\hat{\rho}}{\rho}\right) ds - e^{-2jk\sqrt{\varepsilon_{rc}}z_1} \right\} \tag{25c}$$

where r_2 and r_1 are the outer and inner radius of the the coaxial line, respectively; ε_{rc} is the relative permittivity of the coaxial line and Γ_0 represents the reflection coefficient of the TEM mode at $z=z_1$ (i.e. at $S=S_{inp}$). On the basis of waveguide theory, $\mathbf{H}_{inp} = (j/\omega\mu_0)\nabla\times\mathbf{E}_{inp}$ and therefore the right hand side integral in (23) can be written as

$$\begin{aligned} j\omega\mu_0 \iint_{S_{inp}} \mathbf{T}\cdot(\hat{\mathbf{n}}\times\mathbf{H}_{inp})\, ds = {} & \frac{-jk\sqrt{\varepsilon_{rc}}}{2\pi\,\mu_{rc}\ln(r_2/r_1)} \left\{ \iint_{S_{inp}} \mathbf{T}\cdot\left(\frac{\hat{\rho}}{\rho}\right) ds \right\} \left\{ \iint_{S_{inp}} \mathbf{E}\cdot\left(\frac{\hat{\rho}}{\rho}\right) ds \right\} \\ & + \frac{2jk\sqrt{\varepsilon_{rc}}\, e^{-jk\sqrt{\varepsilon_{rc}}z_1}}{\mu_{rc}\sqrt{2\pi\ln(r_2/r_1)}} \iint_{S_{inp}} \mathbf{T}\cdot\left(\frac{\hat{\rho}}{\rho}\right) ds \ . \end{aligned} \tag{27}$$

Discretization of (23) using tetrahedrals in the volume and triangles on the aperture [17] in conjunction with Galerkin's method yields the system

$$A(k)\, e(k) = g(k) \ , \tag{28a}$$

$$g(k) = \frac{2jk\sqrt{\varepsilon_{rc}}\, e^{-jk\sqrt{\varepsilon_{rc}}z_1}}{\mu_{rc}\sqrt{2\pi\ln(r_2/r_1)}} \iint_{S_{inp}} \mathbf{T}\cdot\left(\frac{\hat{\rho}}{\rho}\right) ds \ . \tag{28b}$$

where $A(k)$ is a partly sparse, partly dense complex symmetric matrix, $g(k)$ is the excitation vector, and $e(k)$ is the unknown electric field coefficient vector. We can express $A(k)$ as the sum of four matrices:

$$A(k) = A_1(k) + A_2(k) + A_3(k) + A_4(k) \ , \tag{29a}$$

$$A_1(k) = \iiint_V \frac{1}{\mu_r}(\nabla \times \mathbf{T}) \cdot (\nabla \times \mathbf{E}) dv - k^2 \varepsilon_r \iiint_V \mathbf{T} \cdot \mathbf{E} \, dv \ , \tag{29b}$$

$$A_2(k) = -2k^2 \iint_{S_{ap}} \mathbf{T}_s \cdot \left(\iint_{S_{ap}} \mathbf{M} \, G_k(R) \, ds' \right) ds \ , \tag{29c}$$

$$A_3(k) = 2 \iint_{S_{ap}} (\nabla \cdot \mathbf{T}_s) \left(\iint_{S_{ap}} (\nabla' \cdot \mathbf{M}) \, G_k(R) \, ds' \right) ds \ , \tag{29d}$$

$$A_4(k) = \frac{jk\sqrt{\varepsilon_{rc}}}{2\pi \, \mu_{rc} \ln(r_2/r_1)} \left\{ \iint_{S_{inp}} \mathbf{T} \cdot \left(\frac{\hat{\rho}}{\rho} \right) ds \right\} \left\{ \iint_{S_{inp}} \mathbf{E} \cdot \left(\frac{\hat{\rho}}{\rho} \right) ds \right\} . \tag{29e}$$

Clearly, the solution of (28) must be repeated for each frequency f. Using the solved fields on S_{inp} (z_1=0) we can compute the reflection

$$\Gamma_0 = \frac{1}{\sqrt{2\pi \ln(r_2/r_1)}} \iint_{S_{inp}} \mathbf{E} \cdot \left(\frac{\hat{\rho}}{\rho} \right) ds - 1 \tag{30}$$

which can then be used for the input admittance evaluation. We have

$$Y_{in} = Y_0 \frac{1 - \Gamma}{1 + \Gamma} \tag{31}$$

where Y_{in} is the input impedance and Y_0=1/Z_0 is the free space admittance. Typically, of interest is the evaluation of Y_{in} over a frequency band. AWE can therefore be employed to achieve this using only a few frequency points. We describe AWE for this application in the next section.

2.3.a Frequency Extrapolation

To apply AWE to the system (28a), we proceed in a similar manner as done in section 2.2.a. The unknown field vector $e(k)$ is again expanded as

$$e(k) = \sum_{n=0}^{\infty} M_n (k - k_0)^n \tag{32a}$$

where the moments M_n given by

$$M_n = A^{-1}(k_0)\left[\frac{g^{(n)}(k_0)}{n!} - \sum_{q=0}^{n} \frac{(1-\delta_{q0})A^{(q)}(k_0)M_{n-q}}{q!}\right] \tag{32b}$$

where $A^{-1}(k_0)$ is the inverse of $A(k_0)$ and for $q>0$, $A^{(q)}(k_0)$ is the q^{th} derivative of the matrix with respect to k evaluated at k_0. Similarly, $g^{(n)}(k_0)$ is the n^{th} derivative of $g(k)$ with respect to k evaluated at k_0. As before, δ_{q0} is the Kronecker delta function defined in (9b). Explicit expressions for the derivatives of $A(k)$ and $g(k)$ are readily obtained and are given by

$$A^{(q)}(k) = \frac{d^q A(k)}{dk^q} = \sum_{m=1}^{4} A_m^{(q)} \ , \ q \geq 0 \ , \ A_m^{(0)}(k) \equiv A_m(k) \ ; \tag{33a}$$

$$A_1^{(1)}(k) = -2k\varepsilon_r \iiint_V \mathbf{T} \cdot \mathbf{E}\, dv \ , \ A_1^{(2)}(k) = A_1^{(1)}(k)/k \ , \ A_1^{(q)}(k) = 0 \ , \ q \geq 3 \ ; \tag{33b}$$

$$A_2^{(1)}(k) = -2\iint_{S_{ap}} \mathbf{T}_s \cdot \left(\iint_{S_{ap}} \mathbf{M}\left[2k - jRk^2\right] G_k(R)\, ds' \right) ds \ , \tag{33c}$$

$$A_2^{(q)}(k) = -2\iint_{S_{ap}} \mathbf{T}_s \cdot \left(\iint_{S_{ap}} \mathbf{M}\, Q_k(R)\, G_k(R)\, ds' \right) ds \ , \ q > 1 \ , \tag{33d}$$

$$Q_k(R) \equiv \frac{q!}{(q-2)!}(-jR)^{q-2} + 2qk(-jR)^{q-1} + k^2(-jR)^q \ ; \tag{33e}$$

$$A_3^{(q)}(k) = 2\iint_{S_{ap}} (\nabla \cdot \mathbf{T}_s) \left(\iint_{S_{ap}} (\nabla' \cdot \mathbf{M}) (-jR)^q G_k(R)\, ds' \right) ds \ , \ q \geq 1 \ ; \tag{33f}$$

$$A_4^{(1)}(k) = A_4(k)/k \ , \ A_4^{(q)}(k) = 0 \ , \ q \geq 2 \ ; \tag{33g}$$

$$g^{(n)}(k) = \left(- j\sqrt{\varepsilon_{rc}} z_1 \right)^n \left[1 - \frac{n}{jk\sqrt{\varepsilon_{rc}} z_1} \right] g(k) \ , \ n \geq 0 \ . \tag{33h}$$

As done in 2.2.a, once the AWE moments are obtained, the electric field coefficients at frequencies around the expansion frequency can be calculated by using (32a). This expansion or its Padè equivalent can in turn be used to compute the frequency response of antenna parameters.

3. Numerical Results

In this section we present some numerical results to demonstrate the accuracy and efficiency of the AWE implementation in connection with MoM and hybrid FEM/MoM techniques. First, as frequency extrapolation applications, scattering by three-dimensional metallic bodies (a PEC plate, a three-PEC plate, a PEC ring) and radiation by a circular patch are examined. We then consider scattering by a metallic plate as an example of pattern fill implementation. Note that all numerical computations for the results presented here were done on an SGI-Indigo2 machine (150 MHz, IP22 processor).

3.1 Frequency Extrapolation

We present below four frequency extrapolation examples, one radiation and three scattering problems. For the latter, the incident plane wave is edge-on incidence and only the monostatic (backscattering) case is considered, that is, α=90°, θ^{inc}= θ^{scat}=90°, and ϕ^{inc}=ϕ^{scat} =0°.

A. PEC Plate

Figure 1 illustrates a metallic plate with dimensions 1 cm x 1 cm. This square PEC plate was discretized using triangular patches, thus yielding 603 unknowns. As a result, the dense full matrix of the MoM system was 603x603 in size. The RCS frequency response was calculated at 30 GHz and this was used as the expansion frequency to generate Pade approximations with L=M=1,2,3,4 in the frequency range 25-35 GHz. As shown in Figure 2, for L=M > 1, the convergence of this expansion is easily achieved. In Figure 3, the RCS frequency response is plotted for the MoM solution, Taylor series expansion with a order of 6, and Pade approximation with L=M=3. As seen, the AWE solution is in good agreement with the exact solution. It is also observed that away from the expansion point, the deviation from the exact response becomes apparent for the Taylor series solution. The Pade approximation with L=M=4 calculated at 0.1 GHz frequency increments resulting in 100 frequency calculations. In fact, AWE can virtually generate the response at any fine increment with almost no cost. The AWE computations were carried out in only 28 minutes while the exact MoM solution for 11 frequencies took 59 minutes (Table 2). This comparison proves that AWE can result in saving at least one half of the CPU time required for the exact solution.

B. Three-PEC Plate

In Figure 4, a configuration of three PEC plates is depicted with dimensions specified in terms of the wavelengths (λ_i, i=1,2,3) at the corresponding frequencies (f_1=3 GHz, f_2=5 GHz, f_3=7 GHz). For this geometry, the number of unknowns was 448 and the system matrix was therefore 448x448 in size. Pade approximations with L=M=1,2,..,7 were obtained in the frequency range 1-9 GHz by expanding the exact solution about 5 GHz. Figures 5 and 6 show the convergence of Pade expansion. As seen, after L=M=5, the Pade solution converges and it agrees with the exact solution very well. However, Taylor series solution diverges as seen in Figure 7. In contrast to the Pade solution, as the order of expansion increases, the Taylor solution severely deteriorates as going away from the expansion point. Although both Pade and Taylor expansions use the same set of moments, the Taylor series fails to extract the dominant poles and residues of the system, unlike the Pade approximation, and therefore any additional term in the series representation does not improve the convergence of the solution. Table 3 shows the CPU comparison of AWE and exact solutions. As seen, the exact solution took 88 minutes for 17 frequency points. However, the Pade approximation with L=5 and M=4 at 80 frequencies was calculated in 19 minutes, which is about one fifth of the MoM solution time. This result demonstrates noticeable performance of AWE in terms of CPU time savings.

C. PEC Ring

A metallic ring with inner radius and thickness of 3 cm and 0.3 cm, respectively, is shown in Figure 8. The number of unknowns for this case was 425, yielding a dense full system matrix of 425x425 in size. Pade approximations with L=M=4 were generated using multiple expansion points in order to recover the RCS response in the frequency band of 1-9 GHz. Figure 9 shows the Pade solution obtained using four expansion frequencies: f_1=2 GHz, f_2=4 GHz, f_3=6 GHz, and f_4=8 GHz. The exact solution at each expansion point was used to extrapolate the solution in the corresponding frequency band designated by vertical lines as shown in Figure 9. These expansions frequencies and frequency bands in which the Pade approximations bmatch with the exact solution as optimum as possible were determined using the basic idea of the complex frequency hopping (CFH) algorithm [18]. As seen, the AWE solution again agrees very well with the exact MoM solution. For the CPU timing comparison as shown in Table 4, the frequency band (2.3-5.3 GHz) with the expansion frequency 4 GHz was chosen. The AWE solution for 30 frequency points was obtained in 18 minutes. On the other hand, in order to recover RCS response properly in that band, we needed to run the MoM code for 10 frequencies in that band, resulting in the CPU time of 44 minutes. This result again shows computational efficiency of the AWE implementation.

D. Circular Microstrip Patch Antenna

A cavity-backed circular microstrip antenna radiating into an infinite ground plane is shown in Figure 10. The input plane S_{inp} is placed at z=0 plane and the radiating aperture at z=0.16 cm. The discretization of the cavity volume resulted in 6,325 unknowns of which 469 were on the aperture. Thus, the dense submatrix was 469x469 in size. The frequency response of the input impedance is calculated at 6 GHz and this was used as the expansion frequency to construct a Padè approximation with L=3 and M=2. The frequency response from 5 GHz to 7 GHz is plotted in Figure 11. As seen, a very good agreement is obtained between the Padè approximation and the exact solution over the frequency range. The Padè expansion was calculated at 0.01 GHz frequency increments resulting in 200 AWE frequency calculations. These were carried out in only 44 minutes whereas direct calculation of the input impedance at 13 frequencies required 5 hours as shown in Table 4. This comparison clearly demonstrates the distinct advantage of AWE for generating broadband frequency responses.

3.2 Pattern Fill

In this section we present an example of pattern fill application described in section 2.2.b. Figure 12 shows a square PEC plate (λ_0 x λ_0) upon which a plane wave with edge-on incidence is impinged. In this case, the order of the system was 408. The monostatic scattering pattern at a fix ϕ=0 cut was calculated by Pade approximations with L=M=2 and L=M=1 using three expansion angles of incidence, θ^{inc}=15°,45°,70°. As seen in

Figure 13, each expansion best approximates the exact RCS pattern in the corresponding angular sector.

4. Conclusions

In this paper, we presented the implementation of the AWE technique in connection with the frequency domain EM methods, namely MoM and hybrid FEM/MoM. AWE was employed as a frequency or an angular extrapolator in this implementation for the purpose of generating broadband frequency or angular reponses, respectively, using only a few of exact solutions. The formulation of this analysis was first time introduced. We presented some representative numerical results for scattering and radiation by three-dimensional configurations to demonstrate the computational efficiency as well as the accuracy of the implementation. As observed from these results, AWE can generate the broadband responses quite accurately with a considerable CPU time saving. As expected, the Pade approximation brings about much reliable representation of these characteristics due to its larger circle of RoC when compared to the Taylor series expansion. In particular, using AWE for pattern fill applications will have the advantage of CPU time saving provided an iterative solver is used.

Acknowledgement

The authors would like to thank Dr. Jian Gong for his invaluable discussions at the beginning steps of the formulation of the analysis.

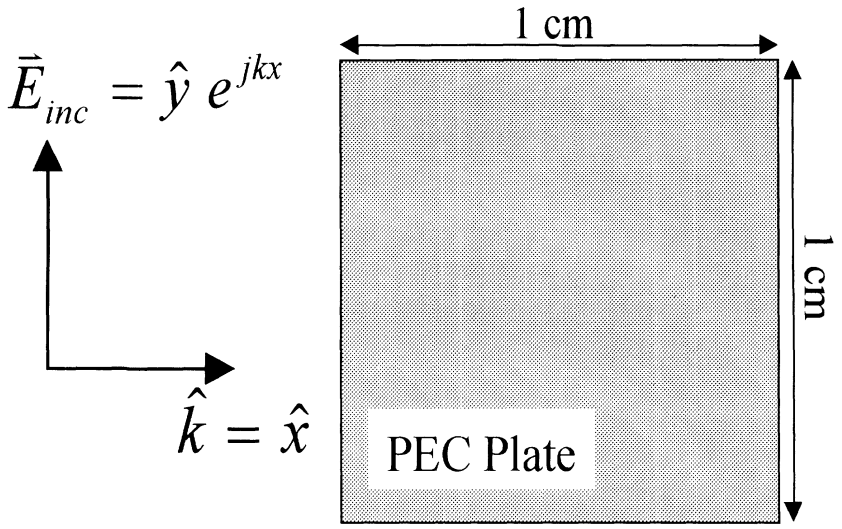

Figure 1 : Metallic square plate; edge-on incidence.

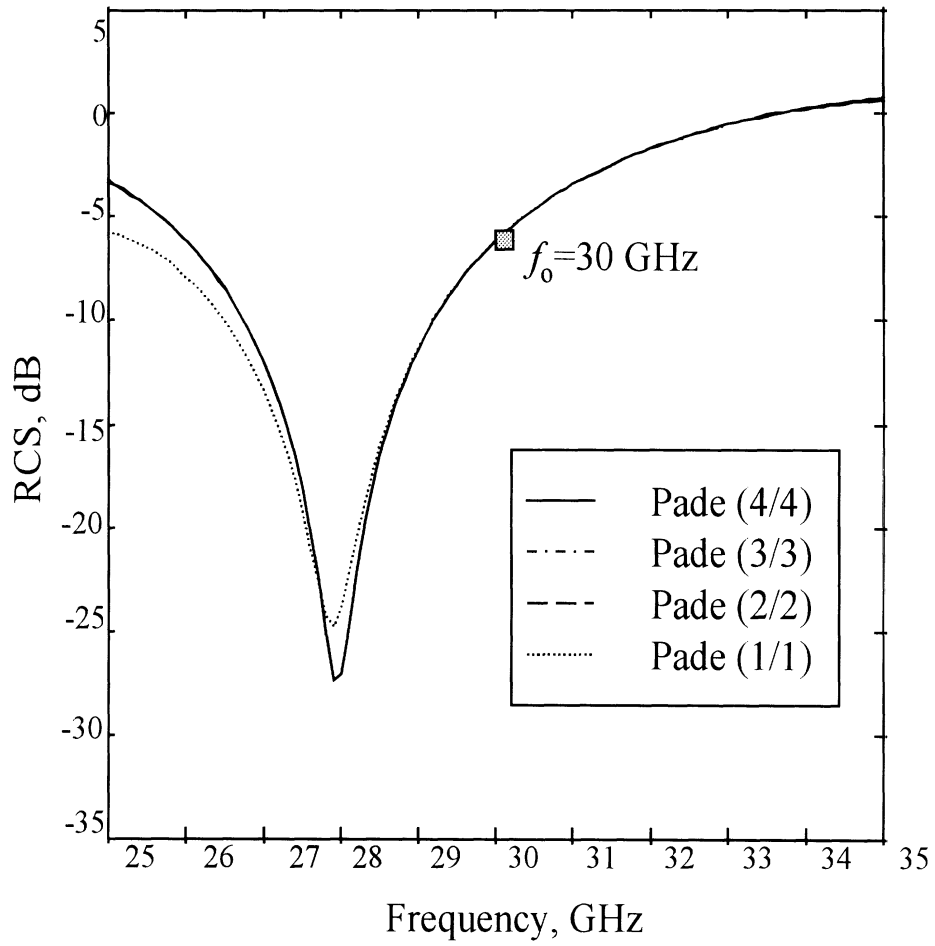

Figure 2 : PEC plate; convergence of Padè solution (L=M=1,2,3,4); expansion frequency, f_0=30 GHz.

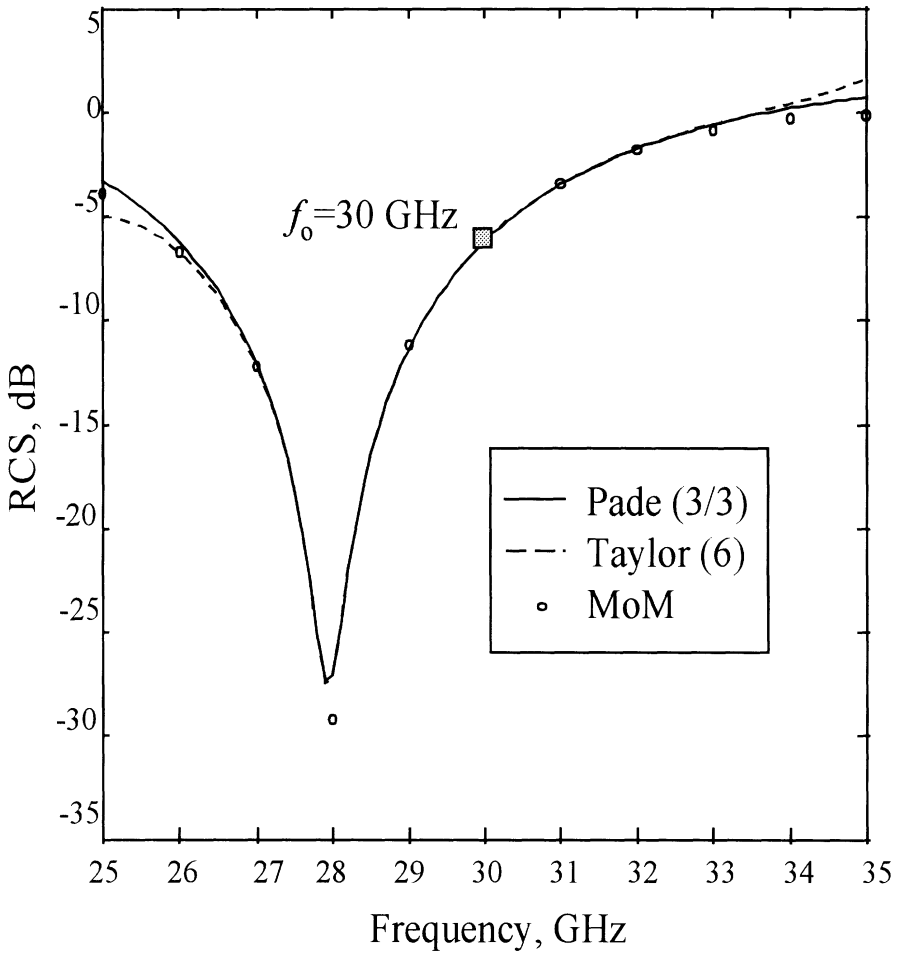

Figure 3 : PEC plate; MoM vs. AWE: Padè(L=M=3), Taylor(6) .

Problem	**Method**	**Matrix Fill** *(secs)*	**LU Factor** *(secs)*	**Total Time** *(secs)*
PEC Plate	MoM (11 freq. points)	3,333	187	3,520
Frequency band 25-35 GHz (f_0=30 GHz)	Padé Approximation (L=M=4) (100 freq. points)	1,672	17	1,689

Table 1 : CPU timings of MoM and AWE solutions for the square PEC plate.

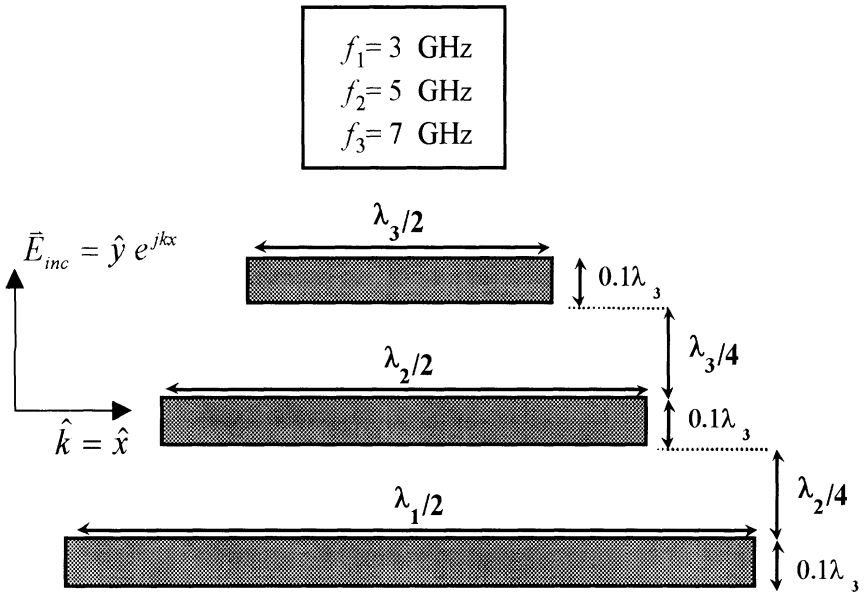

Figure 4 : Three-PEC plate; edge on incidence.

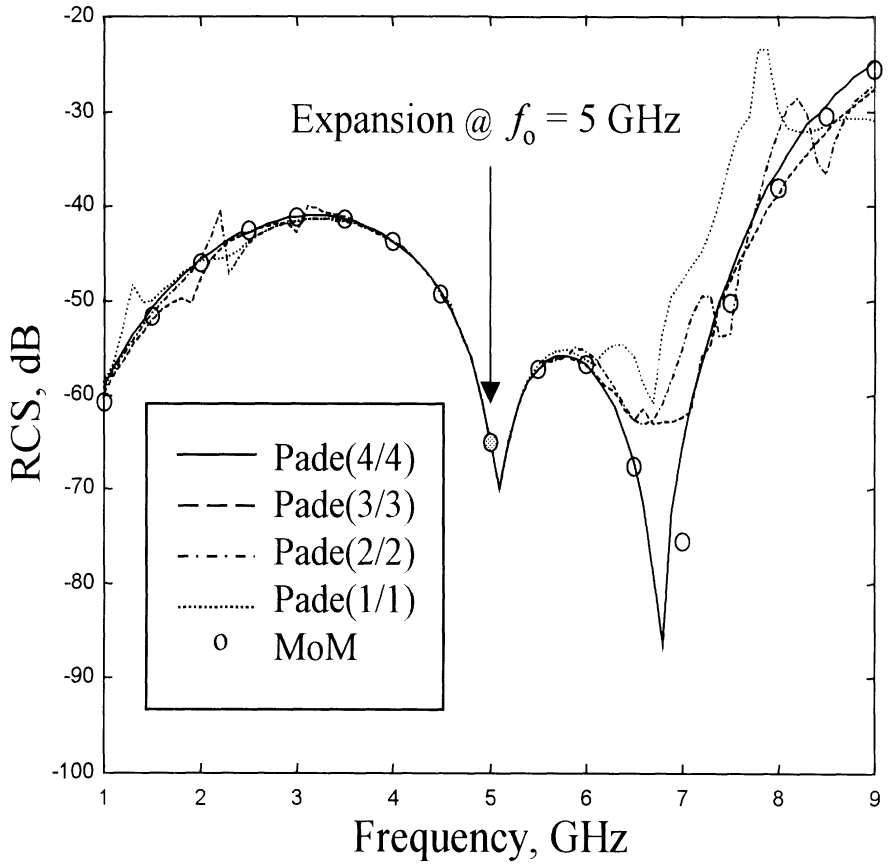

Figure 5 : 3-PEC plate; convergence of Padè solution; expansion frequency, f_0=5 GHz. MoM vs. Padè (L=M=1,2,3,4).

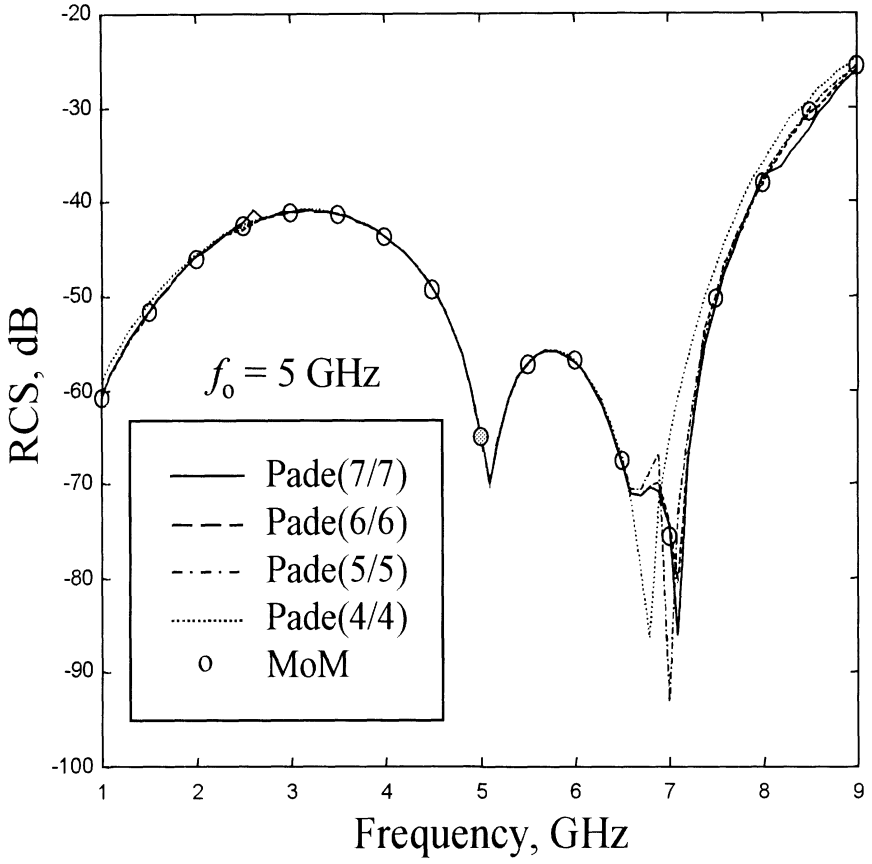

Figure 6 : 3-PEC plate; convergence of Padè solution; expansion frequency, f_0=5 GHz. MoM vs. Padè (L=M=4,5,6,7).

Problem	**Method**	**Matrix Fill** *(secs)*	**LU Factor** *(secs)*	**Total Time** *(secs)*
3-PEC plate	MoM (17 freq. points)	5,168	119	5,287
Frequency band 1-9 GHz (f_0=5 GHz)	Padé Approximation (L=5, M=4) (80 freq. points)	1,110	7	1,117

Table 2 : CPU timings of MoM and AWE solutions for the 3-PEC plate problem.

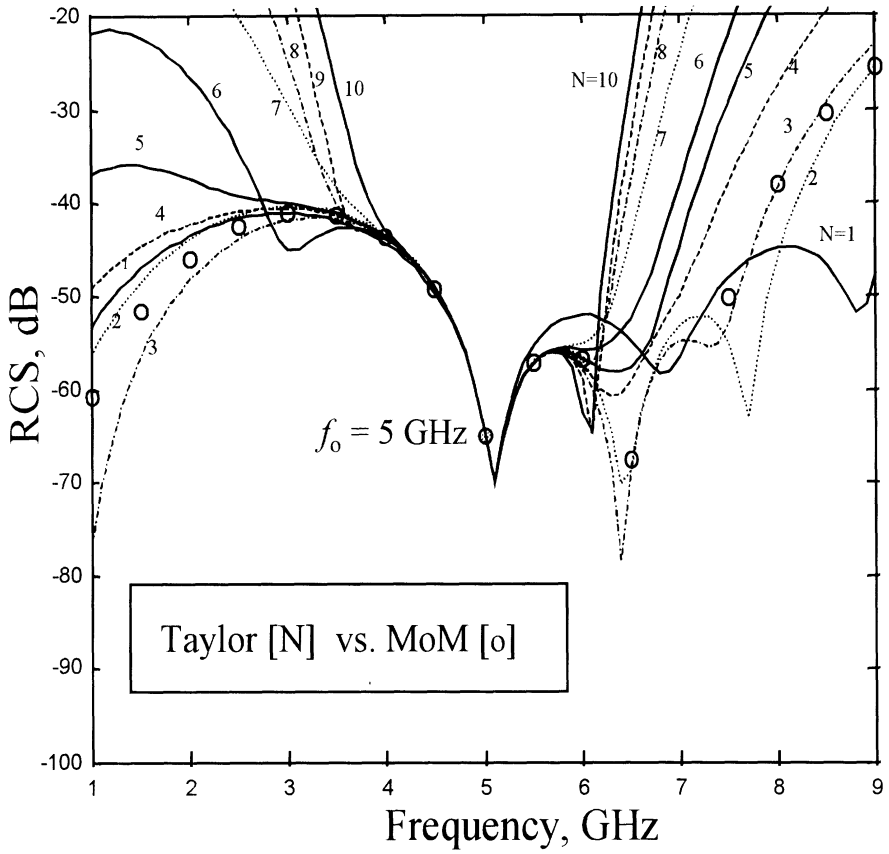

Figure 7 : 3-PEC plate; divergence of Taylor solution; expansion frequency, f_0=5; MoM vs. Taylor (N=1,2,...,10).

Problem	**Method**	**Matrix Fill** *(secs)*	**LU Factor** *(secs)*	**Total Time** *(secs)*
PEC Ring	MoM (10 freq. points)	2,570	50	2,620
Frequency band 2.3-5.3 GHz (f_0=4 GHz)	Padé Approximation (L=M=4) (30 freq. points)	1,097	5	1,102

Table 3 : CPU timings of MoM and AWE solutions for the PEC ring problem.

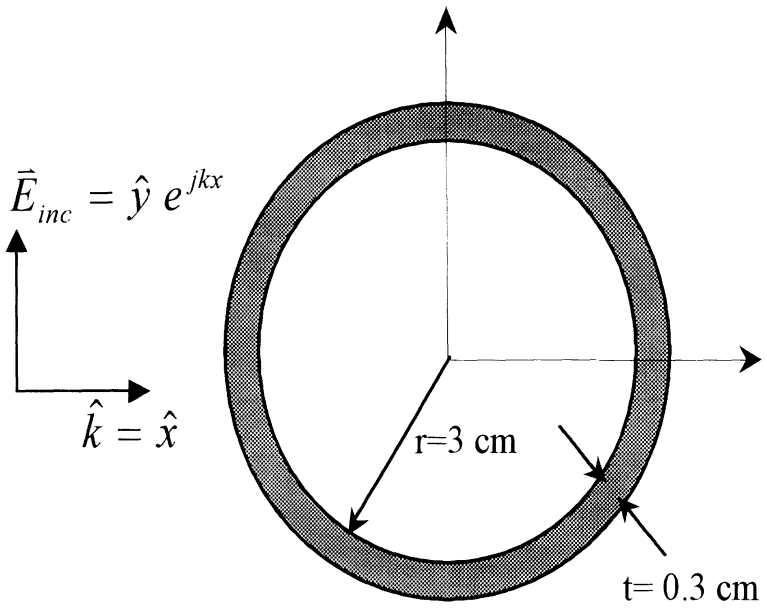

Figure 8 : PEC ring; edge-on incidence.

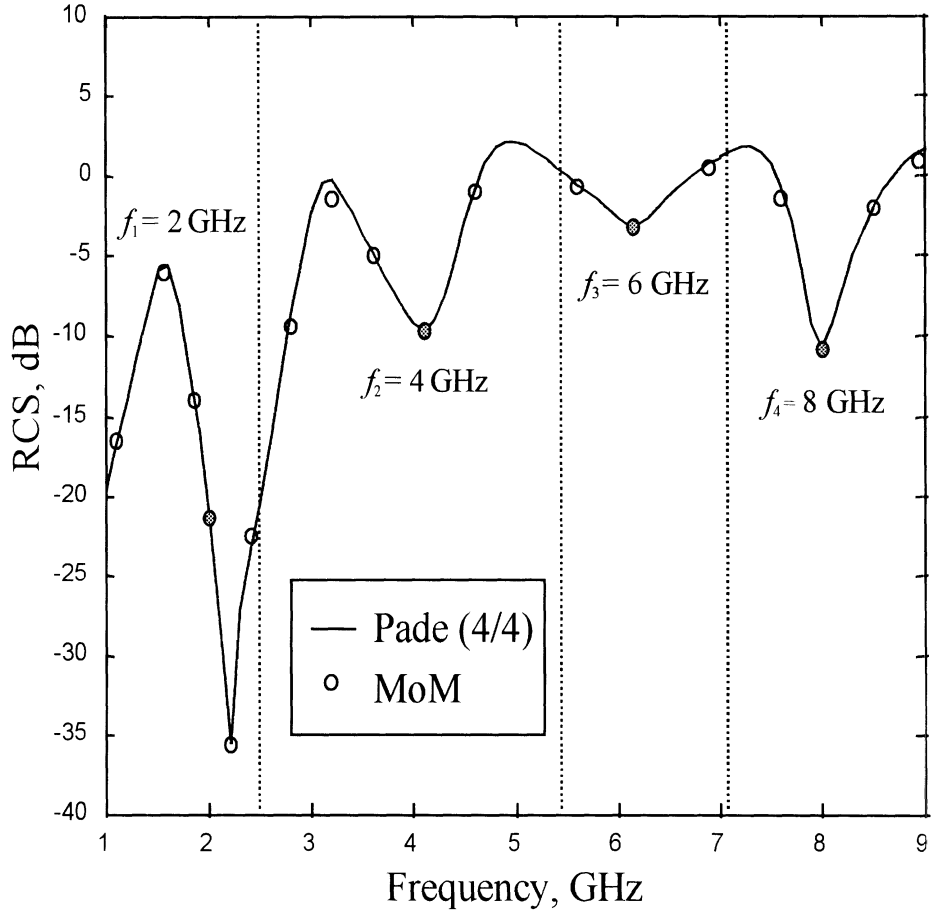

Figure 9 : PEC ring; MoM vs. Padè (L=M=4) approximation using multiple expansion points, f_1=2 GHz, f_2=4 GHz, f_3=6 GHz, f_4=8 GHz.

Problem	Method	Matrix Fill *(secs)*	LU Factor *(secs)*	Total Time *(secs)*
Circular Microstrip Patch Antenna	Hybrid FEM/MoM (13 freq. points)	16,900	1,144	18,044
Frequency band 5-7 GHz (f_0=6 GHz)	Padé Approximation (L=3, M=2) (200 freq. points)	2,535	88	2,623

Table 4 : CPU timings of FE/MoM and AWE solutions for the circular microstrip patch antenna problem.

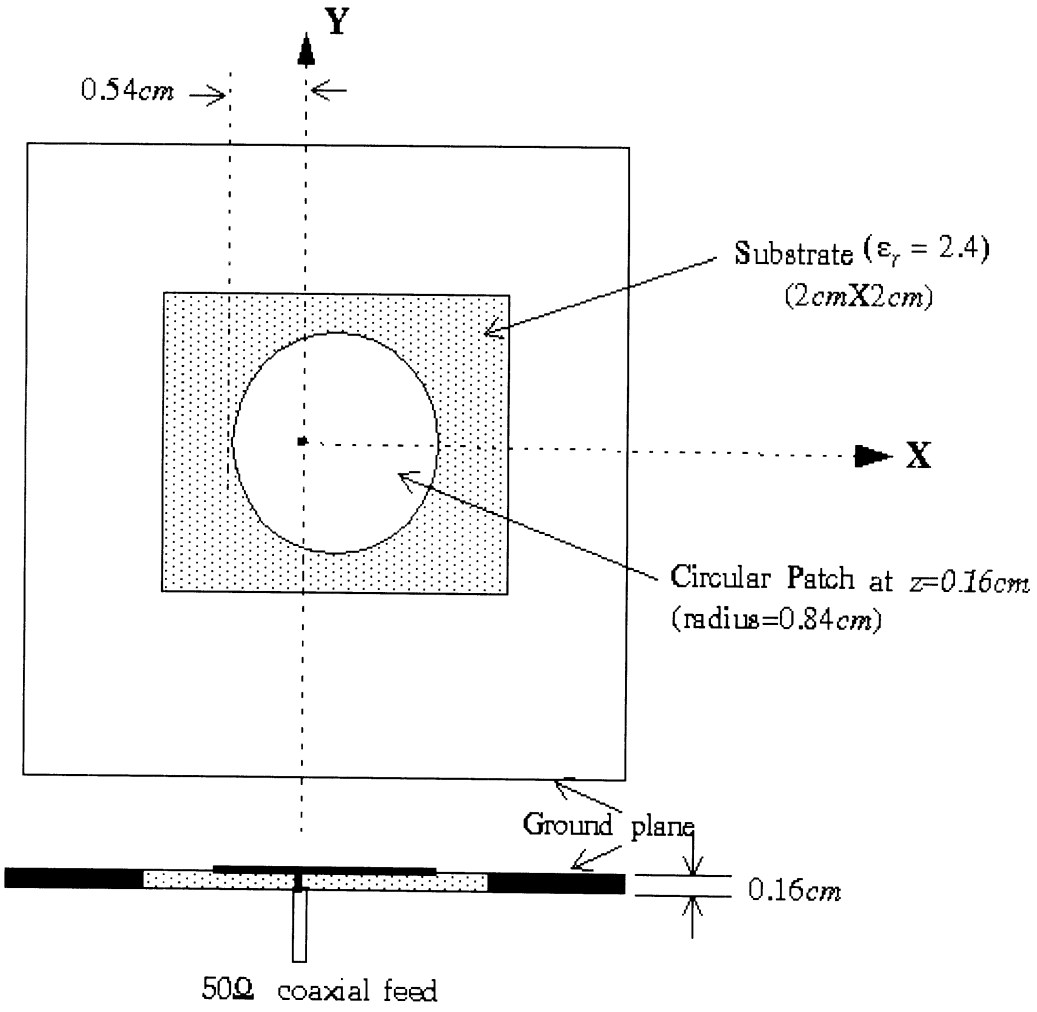

Figure 10 : Cavity-backed circular microstrip patch antenna.

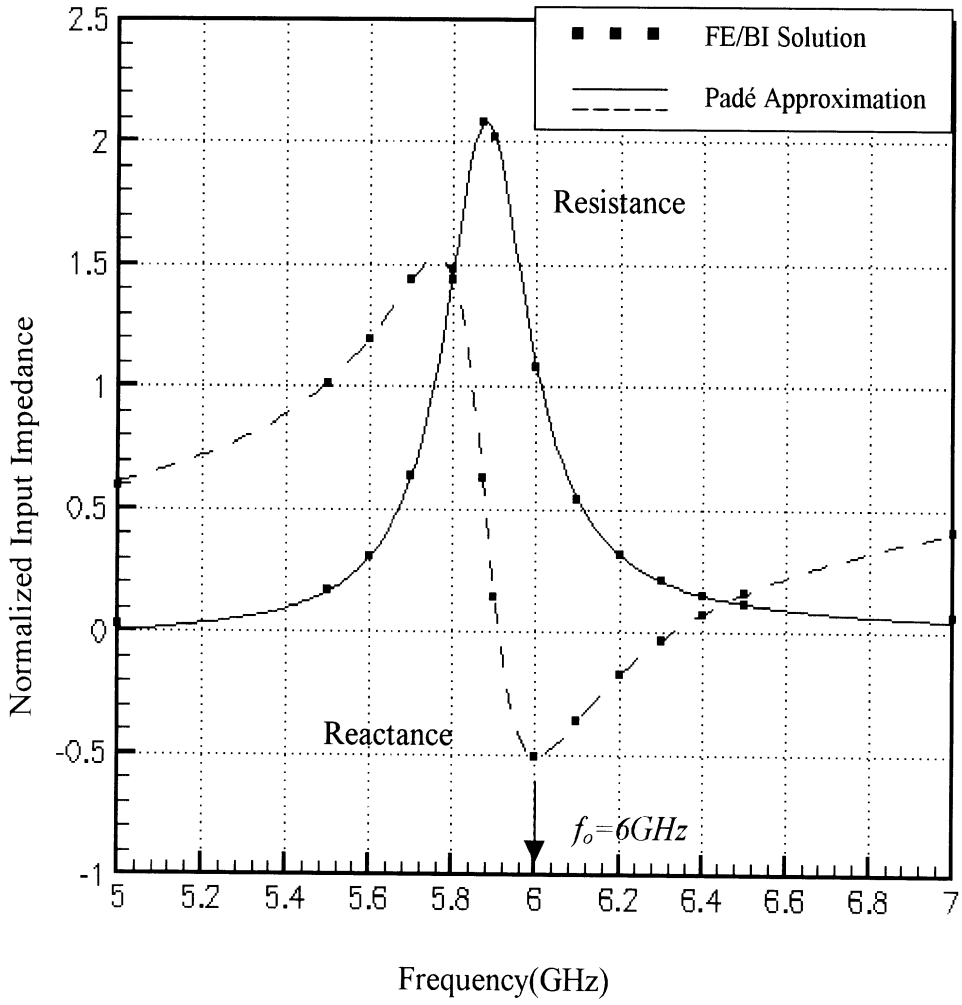

Figure 11 : Normalized input impedance of a cavity-backed circular microstrip patch antenna.

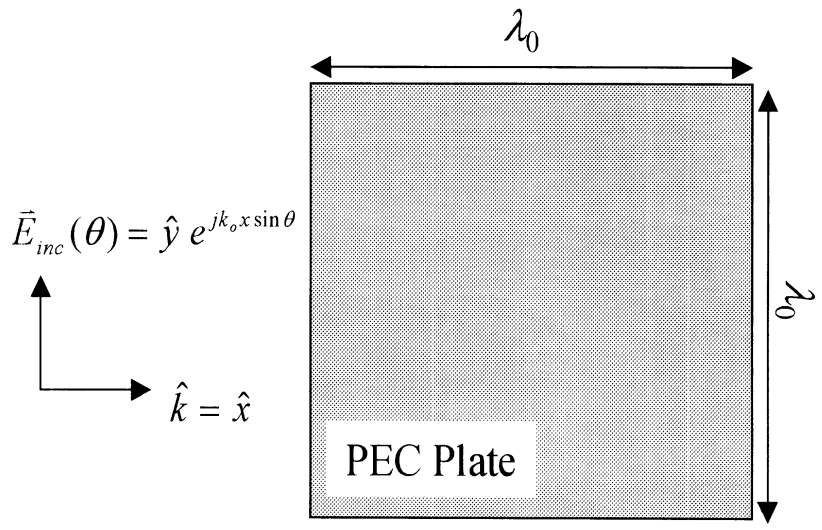

Figure 12 : Metallic square plate.

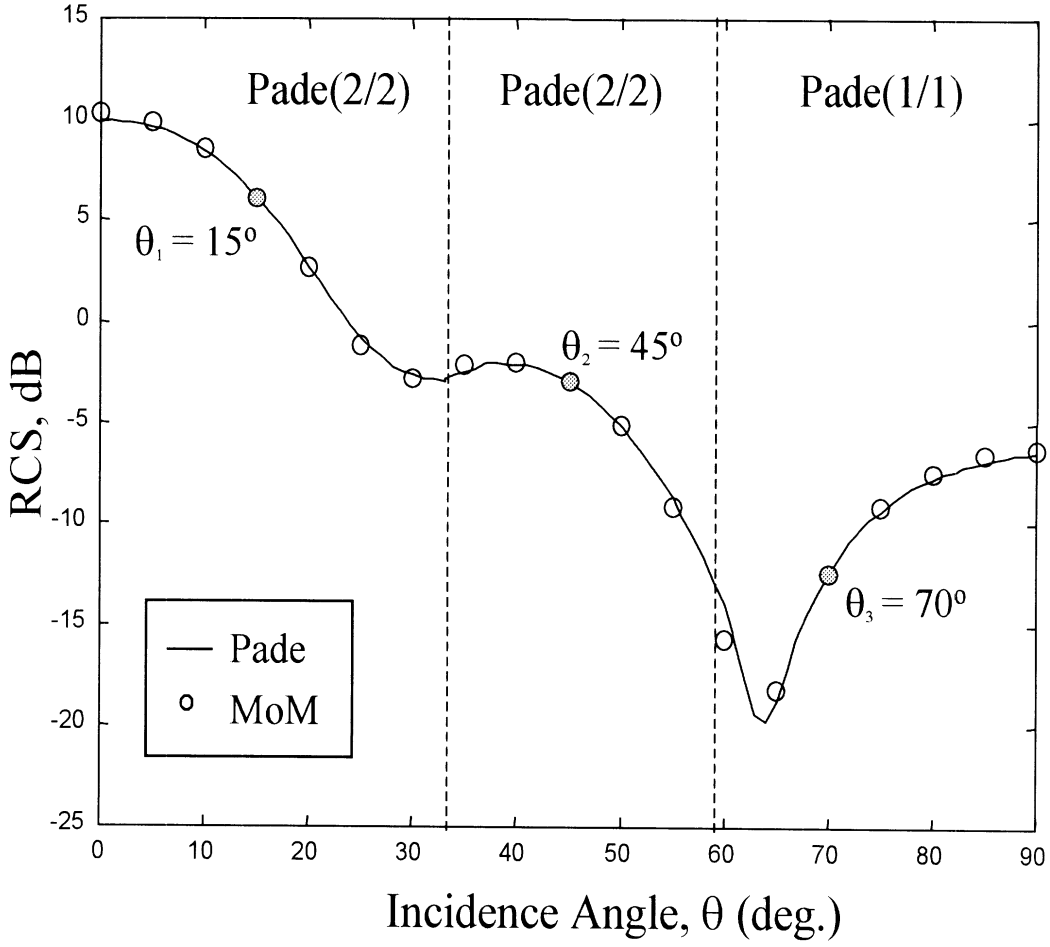

Figure 13 : PEC plate; pattern fill using multiple expansion points, θ_1=15°, θ_2=45°, θ_3=70°. MoM vs.Padè (L=M=2 and L=M=1).

References:

[1] E. K. Miller, L. Medgysi-Mitschang, and E. H. Newman (Eds), *Computational Electromagnetics: Frequency Domain Method of Moments*, IEE Press, New York, 1992.

[2] J. L. Volakis, A. Chatterjee, and J. Gong, "A class of hybrid finite element methods for electromagnetics: A review," *J. Electromagn. Waves Applications*, vol. 8, no. 9/10, pp. 1095-1124, 1994.

[3] R. Coifman, V. Rokhlin, and S. Wandzura, "The fast multipole method for the wave equation: A pedestrian prescription," *IEEE Antennas and Propagation Magazine*, vol. 35, no. 3, pp. 7-12, 1993.

[4] E. Bleszynski, M. Bleszynski, and T. Jaroszewicz, "AIM: Adaptive integral method for solving large-scale electromagnetic scattering and radiation problems," *Radio Science*, vol. 31, no. 5, pp. 1225-1251, 1996.

[5] J. Song, C. C. Lu, and W. C. Chew, "Multilevel fast multipole algorithm for electromagnetic scattering by large complex objects," *IEEE Transactions on Antennas and Propagation*, vol. 45, no. 10, pp. 1488-1493, 1997.

[6] S. S. Bindiganavale and J. L. Volakis, "A hybrid FEM-FMM technique for electromagnetic scattering," *IEEE Transactions on Antennas and Propagation*, vol. 45, no. 1, pp. 180-181, 1997.

[7] S. S. Bindiganavale, *Fast memory saving algorithms for electromagnetic scattering and radiation*, Ph.D. Thesis, University of Michigan, August 1997.

[8] S. Kumashiro, R. Roherer, and A. Strojwas, "Asymptotic waveform evaluation for transient analysis of 3-D interconnect structures," *IEEE Transaction on Computer-Aided Design of Integrated Circuits and Systems*, vol. 12, no. 7, pp. 988-996, 1993.

[9] E. Chiprout and M. Nakhla, *Asymptotic Waveform Evaluation and moment matching for interconnect analysis*, Norwell Kulwar Acad Publications, 1994.

[10] G. J. Burke, E. K. Miller, S. Chakrabarthi and K. Demarest, "Using model-based parameter estimation to increase the efficiency of computing electromagnetic transfer functions," *IEEE Trans. Magnetics*, vol. 25, pp. 2807-2809, 1989.

[11] E. K. Miller and G. J. Burke, "Using model-based parameter estimation to increase the physical interpretability and numerical efficiency of computational electromagnetics," *Computer Physics Communications*, vol. 68, pp. 43-75, 1991.

[12] J. Gong and J. L. Volakis, "AWE implementation for electromagnetic FEM analysis," *Electronics Letters*, vol. 32, no. 24, pp. 2216-2217, 1996.

[13] S. V. Polsytyanko, R. Dyczij-Edlinger, J. F. Lee, "Fast frequency sweep technique for the efficient analysis of dielectric waveguides," *IEEE Transactions on Microwave Theory and Techniques,* vol. 45, no. 7, pp. 1118-1126, 1997.

[14] G. A. Baker, Jr. and P. Graves-Morris, *Encyclopedia of Mathematics and Its Applications: Padè Approximants, Part I: Basic Theory*, vol. 13, Addison-Wesley Pub. Co., Massachusetts, 1981.

[15] S. M. Rao, D. R. Wilton, and A. W. Glisson, "Electromagnetic scattering by surfaces of arbitrary shape," *IEEE Transactions on Antennas and Propagation*, vol. 30, no. 5, pp. 409-418, 1982.

[16] J. L. Volakis, T. Ozdemir, and J. Gong, "Hybrid finite-element methodologies for antennas and scattering," *IEEE Transactions on Antennas and Propagation*, vol. 45, no. 3, pp. 493-507, 1997.

[17] J. Gong, J. L. Volakis, A. C. Woo, and H. T. Wang, "A hybrid finite element-boundary integral method for the analysis of cavity-backed antennas of arbitrary shape," *IEEE Transactions on Antennas and Propagation*, vol. 42, no. 9, pp. 1233-1242, 1994.

[18] M. A. Kolbehdari, M. Srinivasan, M. S. Nakhla, Q. J. Zhang, and R. Achar, "Simultaneous time and frequency domain solutions of EM problems using finite element and CFH techniques," *IEEE Transactions on Microwave Theory and Techniques,* vol. 44, no. 9, pp. 1526-1534, 1996.